# Measurement of the $^{16}N(2^-,g.s.)\rightarrow{}^{16}O(0^+,g.s.)+e^-+\bar{\nu}_e$ beta-decay branching ratio

Alexandra R. Heath and Gerald T. Garvey
*Argonne National Laboratory, Argonne, Illinois 60439*
*and University of Chicago, Chicago, Illinois 60637*
(Received 13 September 1984; revised manuscript received 11 March 1985)

The $^{16}N(2^-,g.s.)\rightarrow{}^{16}O(0^+,g.s.)+e^-+\bar{\nu}_e$ branching ratio is remeasured. A flatfield magnetic spectrometer, instrumented with a multiwire position-sensitive proportional detector, is used. A value for the branching ratio $\Gamma_\beta(2^-\rightarrow 0^+)/\Gamma_\beta(2^-)=0.2811\pm0.0064$ is determined. Combining this result with another recent determination produces a best value for this branching ratio. This in turn allows a more precise determination of the beta-decay rate ($\Lambda_\beta$) for the process $^{16}N(0^-$, 120 keV$)\rightarrow{}^{16}O(0^+,g.s.)+e^-+\bar{\nu}_e$. A value $\Lambda_\beta(0^-\rightarrow 0^+)=0.489\pm0.020$ sec$^{-1}$ is obtained, which agrees with calculation only when pion exchange currents are included in the nucleon axial current.

## I. INTRODUCTION

The existence of virtual mesons in nuclei implies that they will contribute to weak and electromagnetic processes. These mesonic contributions are usually small and difficult to identify with certainty. The obstacles to their observation are twofold: (1) the experiments are usually difficult, and (2) the nuclear wave functions employed are not sufficiently accurate. Considerable progress, however, has been made in characterizing pion exchange currents because (1) they are usually the largest exchange currents and (2) the small mass of the pion does not lead to undue sensitivity to the wave function at small internucleon distances.

In the impulse approximation the axial vector current is given by $\bar{\psi}(\gamma_\mu\gamma_5\tau_\pm)\,\psi$, where $\bar{\psi}$ and $\psi$ are individual nucleon wave functions. The timelike part of this current is order $p/m$ while the space part is order 1. If a pion is present at the axial vertex the current appears vectorlike and hence has a time component of order 1 and a space component of order $p/m$. On the basis of this simple kinematic consideration one expects that pionic meson exchange currents (MEC's) would have maximal effect in processes where the timelike part of the axial current either dominates or can be readily isolated. These arguments were first put forth in the late seventies by Kubodera, Delorme, and Rho[1] (KDR) and Guichon, Giffon, and Samour.[2]

An ideal transition for isolating this weak axial charge density is $J^\pi=0^-\leftrightarrow J^\pi=0^+$. In this case, the leading order matrix elements in the nonrelativistic impulse approximation are the axial vector time component, $\langle\boldsymbol{\sigma}\cdot\mathbf{p}/m\rangle$, and the first forbidden matrix element, $\langle\boldsymbol{\sigma}\cdot k\mathbf{r}\rangle$, arising from the space component coupled to one unit of lepton angular momentum. An especially attractive case in light nuclei is the weak transition between the first excited $J^\pi=0^-$ state of $^{16}N$ and the $0^+$ ground state of $^{16}O$. The two transitions linking these states are

$$^{16}N(0^-,120\text{ keV})\rightarrow{}^{16}O(0^+,g.s.)+e^-+\tilde{\nu}_e \qquad (1)$$

and

$$\mu^-+{}^{16}O(0^+,g.s.)\rightarrow{}^{16}N(0^-,120\text{ keV})+\nu_\mu\,. \qquad (2)$$

These transitions have received a great deal of attention.[1–11] Detailed calculations by Towner and Khanna[9] confirmed the expectation that the beta decay rate would be enhanced insofar as they calculate the beta decay probability ($\Lambda_\beta$) increased by a factor of 3 when the pionic MEC is included.

The muon-capture rate ($\Lambda_\mu$) between these two states has been investigated for many years to extract the induced pseudoscalar coupling constant, $g_p$, in finite nuclei. Calculated values of $\Lambda_\mu$ depend strongly on the value of $g_p$, but unfortunately, also depend upon the details of the wave functions employed in the calculations. Maksymowicz[11] observed that the ratio $\Lambda_\mu/\Lambda_\beta$ remains sensitive to $g_p$, but the sensitivity to parameters of the particular nuclear model he considered was significantly reduced compared to that of the individual rates. The recent "realistic" calculations by Towner and Khanna[9] confirm Maksymowicz's earlier observation, as they find $\Lambda_\mu/\Lambda_\beta$ is relatively stable to a variety of different residual interactions. There have been several measurements of $\Lambda_\mu$; the weighted mean of the most recent two[12,13] gives $\Lambda_\mu=1560\pm94$ sec$^{-1}$.

There are four published measurements of $\Lambda_\beta$.[14–17] All calibrate their beta detector efficiency employing the measured branching ratio of the $^{16}N$ ground state decay to the $^{16}O$ ground state relative to the decays that produce a 6.13 MeV photon. The previous 10.6% uncertainty[18] in this branching ratio limited the accuracy with which the $(^{16}N,0^-)$ to $(^{16}O,0^+)$ decay rate could be measured. For example, the errors in the most accurate measurement[16] of $\Lambda_\beta$ were completely dominated by this error. Apart from the 10.6% error in this calibration the error in the remainder of the measurement[16] is only 4.8%. A precise value for $^{16}N(2^-,g.s.)\rightarrow{}^{16}O(0^+,$ g.s.) branching ratio has recently been determined by Warburton *et al.*[19] This result was achieved by a careful analysis of a much earlier measurement of the spectral shape by Alburger *et al.*[20] They obtain

 

$$\frac{\Gamma_\beta(2^-,\text{g.s.}\rightarrow 0^+,\text{g.s.})}{\Gamma_\beta(2^-)}=0.279\pm0.005\ .$$

The measurement reported below uses a very different technique but is in excellent agreement with this result.

Figure 1 shows the levels and transitions[18] involved in the beta decay of the two lowest-lying states in $^{16}N$.

In the experiment reported on in this paper the branching ratio of the $^{16}N$ ground state decay to the $^{16}O$ ground state is measured by counting a known fraction of the beta particles leading to the $^{16}O$ ground state normalized to the total number of decays of the $^{16}N$ ground state. The total number of decays is measured using a $\beta$-$\gamma$ coincidence technique. For this phase of the measurement the electrons are detected in a thin plastic scintillator, and the $\gamma$ rays from the decay of the 6.13 MeV $^{16}O$ level are detected in a NaI spectrometer. The singles beta and gamma spectra as well as the beta-gamma coincidence spectra are stored with the spectrum of time delays [time-to-amplitude converter (TAC)] between beta and gamma events. As all discriminator settings are common and pulse height levels can be set in software the technique is insensitive to discriminator levels. Since the beta-gamma angular correlation is isotropic, the ratio of the product of individual singles rates to the coincidence rate directly yields the total decay rate. Gamma rays following beta decay to higher states of $^{16}O$ at 7.12 and 8.87 MeV which cascade through the 6.13 MeV level yield the same contribution to the singles gamma spectra as they do to the $\beta\gamma$ coincidence spectra; hence this effect is included. A definite momentum bite of the electrons leading to the $^{16}O$ ground state is measured in a flatfield magnetic spectrometer. The electrons enter the spectrometer through an active collimator, are deflected by 180° in the magnetic field, and detected in a system consisting of a three wire gas proportional counter backed by a plastic scintillator. The overall efficiency of the magnetic spectrometer is determined by calibrating it with the $^{20}F$ decay for which the branching ratio is known to high accuracy.[21]

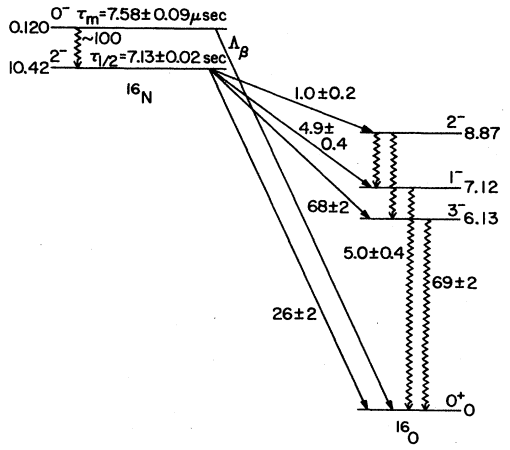


FIG. 1. The levels and transitions (Ref. 18) of the $A=16$ system relevant to $^{16}N$ beta decay. The $^{16}N$ ground-state energy is with respect to $^{16}O$(g.s.). The branching ratios listed are in percent and include the effects of cascades from higher levels.

## II. EXPERIMENTAL APPARATUS

The experimental setup is shown in Figs. 2 and 3. The deuteron beam on the target is defined by two tantalum collimators. The target is at 25° to the beam direction, and produces a 2 mm diam source for the magnetic spectrometer. In the $\beta$-$\gamma$ system used to determine the total number of decays, the $\beta$ detector is a 1.27 cm diam, 0.16 cm thick NE102 plastic scintillator optically epoxied to a Hamamatsu R1213 1.91 cm photomultiplier tube. The $\gamma$ scintillator is a 10 cm diam by 10 cm deep NaI crystal.

The entrance to the beta magnetic spectrograph is defined by an active collimator. The active collimator is a 1.91 cm$\times$1.27 cm, 0.08 cm thick NE102 plastic scintillator with a 2 mm diam hole. It is mounted in a tapered light guide which is coupled to a second Hamamatsu R1213 1.91 cm photomultiplier tube. The purpose of the active collimator is to eliminate effects of slit scattering on the electrons detected in the spectrograph. A measurement of the solid angle subtended by the active collimator was carried out using $^{20}F$ decay and a 300 $\mu$m totally depleted Si detector placed behind the active collimator to count the total number of electrons that pass the collimator without creating observable scintillation. The ratio of the rate of electrons detected in the solid state detector in anticoincidence with the active collimator to the total decay rate as determined by the $\beta$-$\gamma$ coincidence measurements yields the acceptance solid angle of the active collimator. The solid state detector efficiency for detecting electrons is taken as unity and its efficiency for detecting $\gamma$ rays is calculated as less than 0.2%. Figure 4 shows the pulse height spectra from the active collimator and shows excellent separation between events that lose energy in the collimator and those that pass through the 2 mm aperture. Figure 5 shows the acceptance solid angle as a function of the discriminator level set on the pulse height from the active collimator. The data is fitted to a curve of the form $Ax^2+B$ which accounts for the physical size of the aperture plus loss due to poor light collection at the slit edge. The true acceptance angle is taken as the extrapolated value at zero-energy loss. The weighted mean of two measurements yields

$$d\Omega_{sp}=(4.09\pm0.05)\times10^{-5}$$

of $4\pi$. This is in excellent agreement with a direct measurement of the aperture area and the source to aperture distance which yields a result

$$(4.13\pm0.08)\times10^{-5}$$

of $4\pi$.

The magnetic spectrograph (Fig. 3) is a 180° flatfield (dipole) magnet. The pole tips are of soft iron, with a semicircular shape. The gap is 1.905 cm. The maximum and minimum radii of curvature observed by the detector system are 11.6 and 6.1 cm, respectively. This allows a maximum momentum bite of $\Delta P/P_{max}=0.47$. The spectrometer detection system, shown in Fig. 3, consists of three proportional gas counters with position sensitive

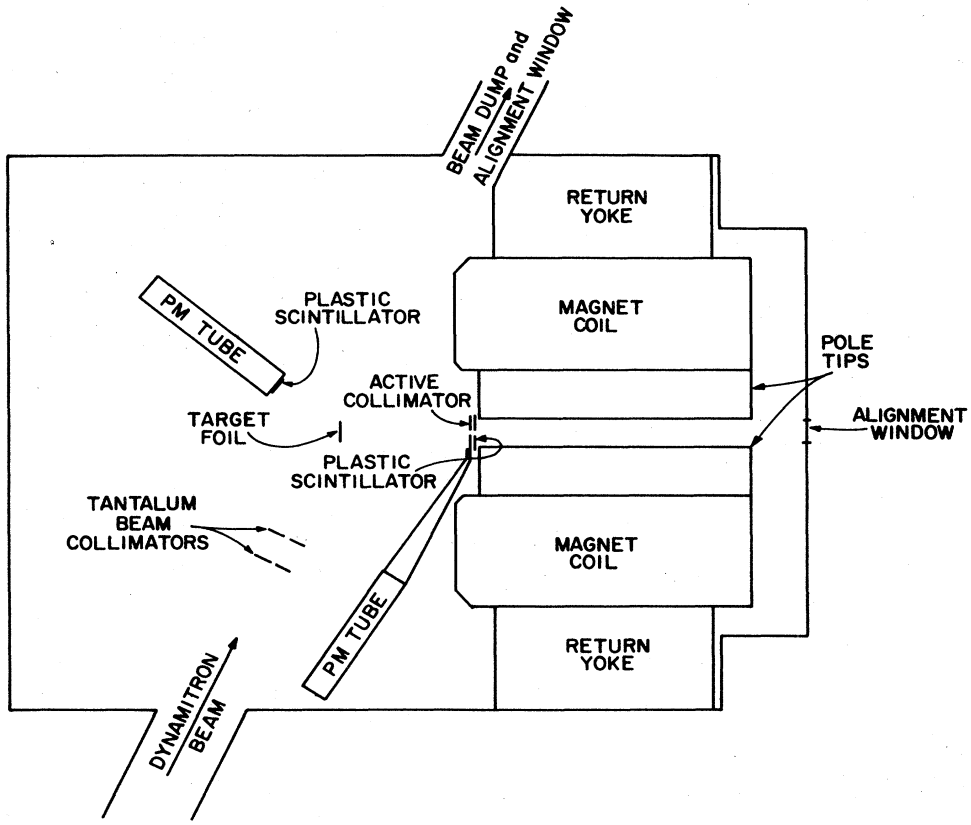


FIG. 2. Plan view of the target chamber, showing the relative locations of the detectors, beam, target, and magnet.

resistive wires. This detector is made up of three chambers of dimensions 6.08 cm high$\times$1.91 cm deep$\times$16.5 cm long. The chambers are parallel to one another and electrically isolated via double aluminized Mylar. The anode wires are 10.3 cm long, 10 $\mu$m diam Moleculoy with a resistivity of 180 $\Omega$/cm. The gas mixture used is P10 (90% argon, 10% methane) at 400 mm pressure regulated via a manostat. The wire detectors are

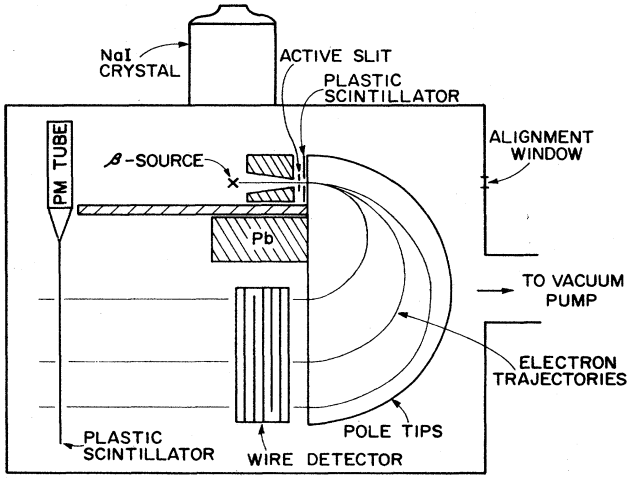


FIG. 3. Elevation view of the target chamber, showing the relative locations of the detectors, target, and magnet.

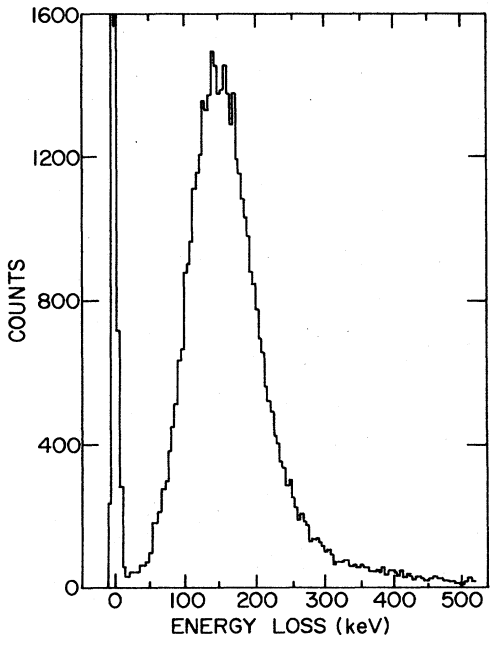


FIG. 4. Typical active slit pulse height spectra taken while observing $^{20}$F decays. The entry scale is set by the peak of the Landau distribution.

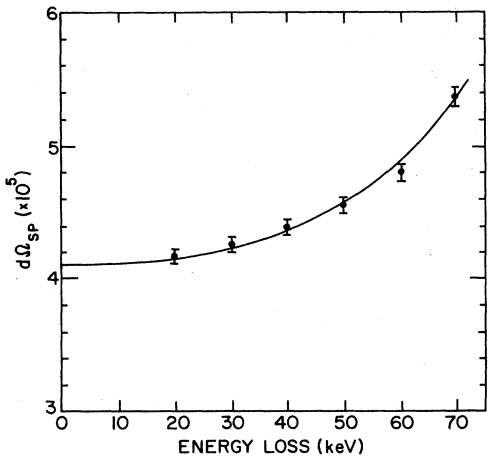


FIG. 5. Active slit acceptance solid angle as a function of the discriminator setting in defining slit anticoincidences. The smooth curve is a two-parameter fit of the form $Ax^2+B$.

backed by a single long thin plastic scintillator (5.08 cm wide $\times$20.3 cm long$\times$0.317 cm thick) located 20 cm behind the wire counter array. The backing plastic scintillator serves both to reject background and to provide a fast timing reference for each of the wires. A good event triggers all three wires, plus the backing scintillator, and produces no signal in the active collimator.

Extensive effort was invested in reducing background in the spectrograph detector system due to the secondary electrons produced by gamma rays. As shown in Fig. 3, lead shielding was inserted between the target and the detection system to reduce the gamma-ray background. Also a thin plastic scintillator, placed behind the active slit, was used to veto any electrons entering the spectrometer other than through the active collimator or its aperture. This scintillator is 1.91 cm wide$\times$7.62 cm long and 0.159 cm thick NE102 with a 0.635 cm diam hole mounted on a light pipe coupled to a Hamamatsu R1213 1.91 cm photomultiplier tube. This additional scintillator further reduced the background by 30%.

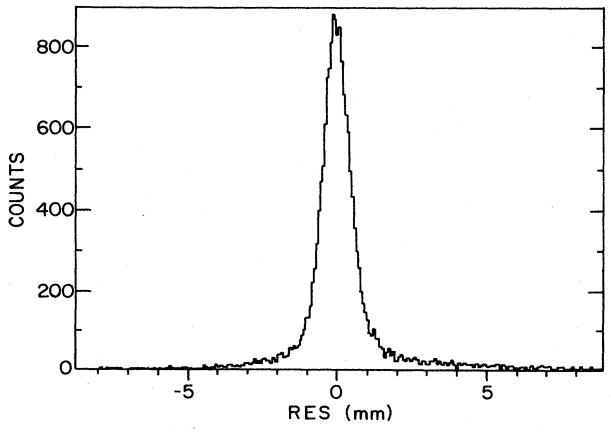


FIG. 6. Typical spectrum of the resolution function RES$\equiv(P1-P2)-(P2-P3)$ taken while observing $^{20}F$ decays.

The pulse height measured at the ends of the wires is used to determine the electron path position along each of the three wires. This allows the angle of incidence of each electron passing through the detector to be determined. The spatial resolution of an electron detector is usually difficult to determine because of the difficulty of obtaining a collimated electron beam or the absence of monoenergetic electron source at sufficient energy. This is the principle reason that the detector was constructed as a three wire system. In this setup any two of the wires can be used to predict the position at the third wire. The spatial resolution of the detector is monitored by constructing a resolution function (RES) defined as RES$\equiv(P1-P2)-(P2-P3)$, where $P1$, $P2$, and $P3$ are the positions along wires 1, 2, and 3, respectively. Figure 6 shows a typical spectrum for the quantity RES. The observed FWHM of RES is observed to be 1.0 mm. No deterioration of resolution due to multiple scattering is expected or observed. If the FWHM of RES is ascribed to electronic noise then the individual resolution of a wire is 0.41 mm assuming that they all have the same magnitude noise level.

In order to remove computer dead time as a possible source of systematic error in this experiment, all events were written on tape through a common gating signal. Thus each event had 19 recorded parameters including a tag which specified it as a gamma ray single, gamma-beta coincidence, electron detected in the magnetic spectrometer, etc. The singles rates from the beta and $\gamma$-ray monitors were prescaled by factors of 100 and 1000, respectively, before being recorded. In addition, the overall dead time losses (0.6%) were monitored by recording the total number of strobes provided to the data acquisition system in a 50 MHz scalar. The strobe rate was typically 50 Hz.

To aid in the identification and correct subtraction of

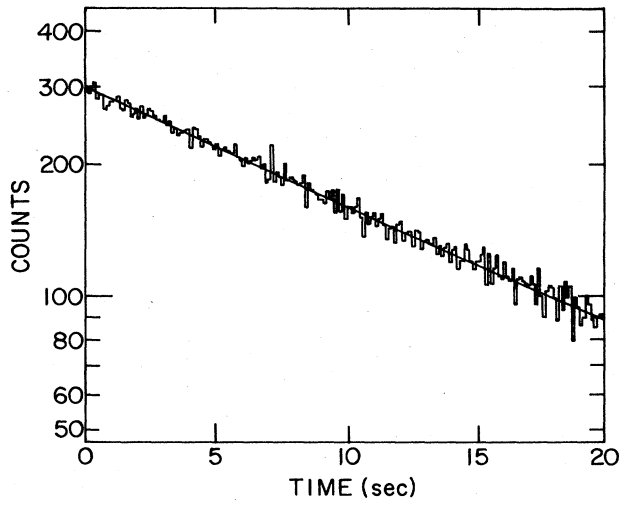


FIG. 7. The observed rate as a function of time, for events in the electron spectrograph ($B=1.625$ kG) with $^6Li^{19}F$ target. The straight line corresponds to a fit with the known lifetime of $^{20}F(\tau_m=15.87\pm0.03$ sec) and no background.

background the elapsed time between beam off and the occurrence of each event was measured in a multiscaling analog-to-digital converter (ADC) and recorded as a parameter. These time decay spectra are well represented by an exponential decay with a constant background. A typical time decay spectrum is shown in Fig. 7.

Both the $^{20}$F and $^{16}$N measurements were run on a 31 sec cycle; the target was irradiated for 10 sec, then the beam was electrostatically deflected, a hold of 1 sec followed by a 20 sec counting period. The $^{20}$F runs were 4–6 h long and the $^{16}$N runs were 6–8 h long. All the data reported herein was accumulated over a 3 d run.

## III. CALIBRATION USING $^{20}$F

The calibration of the efficiency of the magnetic beta spectrometer requires the measurement of a decay with a known branching ratio. The total activity must be counted as well as the fraction detected in the spectrometer. This result can then be applied to the less accurately measured $^{16}$N case.

The beta decay of $^{20}$F($2^+$, g.s.) with a half-life of 11.0±0.02 sec, is known[21] to take place with 99.9% probability to the first excited state of $^{20}$Ne($2^+$, 1.63 MeV) followed by $\gamma$-ray emission to the ground state of $^{20}$Ne($0^+$). The $^{20}$F activity was produced via the $^{19}$F(d,p)$^{20}$F reaction using a 100 nA, 1.7 MeV deuteron beam incident on $^6$LiF(300 $\mu$g/cm$^2$) target with carbon (40 $\mu$g/cm$^2$) backing. Au was evaporated on both sides (230 $\mu$g/cm$^2$ on the front and 350 $\mu$g/cm$^2$ on the back) to ensure that recoiling $^{20}$F nuclei stopped in the target.

The singles electron and 1.63 MeV gamma-ray time decay spectra were found to consist of a component with proper time decay (15.87 sec) and a time independent (long-lived compared to the 20 sec cycle length) component. A two-parameter fit to those spectra of the form $A\exp(-t/\tau_m)+B$, where $\tau_m$ is the proper decay time constant, allows determination of the background present in the singles spectra. In the case of electron singles spectrum the background is due to positrons from the decay of $^{13}$N (half-life of 9.96 min) produced by the (d,n) reaction with the $^{12}$C present in the target backing. The time spectra of the $\beta\gamma$ coincidences and of electrons detected in the magnetic spectrometer were found to consist of only a single component with the proper decay constant. Table I shows the values obtained for $A$ and $B$ for each spectrum.

The momentum calibration of the magnetic spectrograph is obtained using the measured $^{20}$F decay spectrum at four different magnetic field settings. The observed spectra are shown in Fig. 8. To within 1% the transition has an allowed shape.[22] The observed spectra is thus subject to a three parameter ($A_0$,$B_0$,$R_0$) fit of the form

$$N(i)=A_0p^2[E_0-\sqrt{p^2+1}]^2F(Z,p)+B_0$$

with

$$p=0.5871B(R_0+\alpha i)\,,$$

where $i$ is the channel number in the position spectra of a resistive wire and $B$ is the magnetic field setting in kilo-Gauss. The value of $\alpha$ is determined by connecting an electronic pulse at the ends of the wire. The Fermi function $F(Z,p)$ is taken from the tables of Behrens and Janecke.[23] The normalization ($A_0$), the background ($B_0$), and the resistive wire position offset ($R_0$) were fit. The response function of the spectrometer is taken as a Gaussian with the full-width at half-maximum, a quadratic combination of the spectrometer geometrical resolution, and the resolution of the wire detectors. The theoretical spectrum shape convoluted with the response function of the spectrometer is used in the fitting routine. The fit is very insensitive to the parameters of the detection response function. Figure 9 shows a plot of the position offset $R_0$ as determined from the different magnetic field settings; a weighted mean yields $R_0=6.072\pm0.024$ cm.

The background present in the position spectra was determined in two ways. First a 0.635 cm thick Pb stopper was used to block the entrance aperture of the spectrometer, and second, the electron angle through the three-wire detector was used to discriminate against unacceptable trajectories. The electron angle is determined by the difference in position measured on wires one and three

TABLE I. The time spectra observed in each of the detectors in this experiment. The time spectra are all fitted to $Ae^{-t/\tau}+B$ where $\tau$ is the proper decay time constant for either $^{20}$F or $^{16}$N. In cases where the $B$ coefficient is consistent with 0 the value of $A$ is shown with $B$ assumed to be 0.

| Decay | | Beta singles | Gamma singles | Beta-gamma coincidence | Spectrograph |
|---|---|---|---|---|---|
| | | | | | 1.625 kG |
| | $A$ | 30 173±50.5 | 51 791±65.4 | 189.3±3.8 | 445.41±9.6 |
| | $B$ | 1350.3±25.5 | 1875±33.0 | 0.93±1.92 | 2.29±4.8 |
| $^{20}$F | | | | | |
| | $A$ | | | 189.3±1.33 | 445.4±3.3 |
| | $B$ | | | 0 | 0 |
| | | | | | 2.720 kG |
| | $A$ | 38 579±43.6 | 78 666±61.5 | 255.4±3.5 | 321.3±6.4 |
| | $B$ | 5010.9±16.2 | 26.6±21.7 | −2.19±1.12 | 0.76±2.44 |
| $^{16}$N | | | | | |
| | $A$ | | 78 665±31.5 | 255.4±1.77 | 321.3±3.2 |
| | $B$ | | 0 | 0 | 0 |

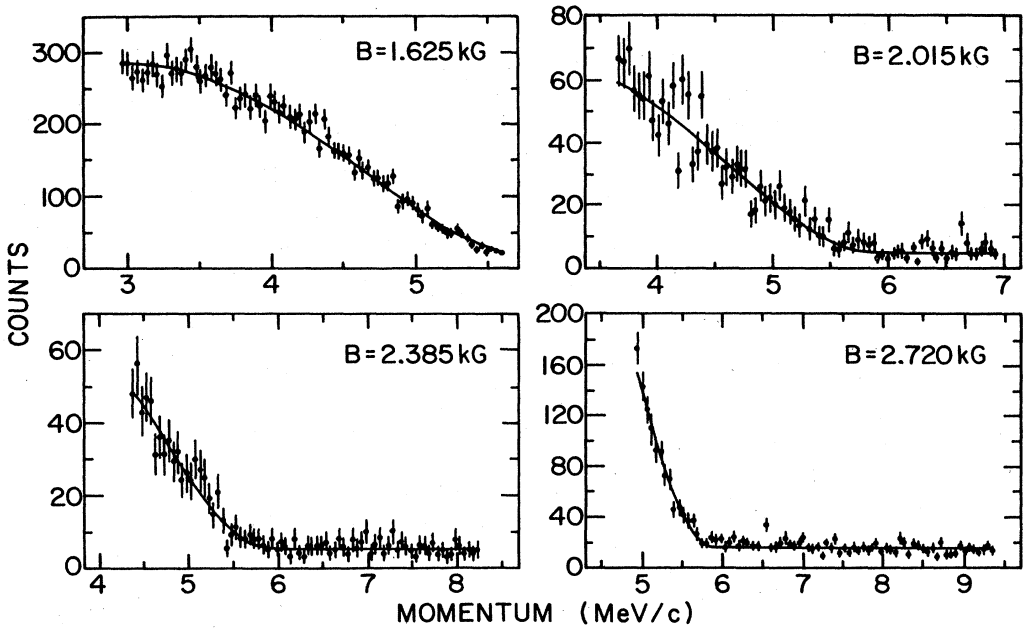


FIG. 8. Position spectra taken for $^{20}F$ decays at different magnetic fields. The smooth curves are three-parameter fits of the form $N(p)=A_0p^2[E_0-\sqrt{p^2+1}]^2F(Z,p)+B_0$ where $p=0.5871B(R_0+\alpha i)$. We fit the normalization $A_0$, the background $B_0$, and the position offset $R_0$.

divided by the 3.81 cm physical separation between the wires. The upper half of Fig. 10 shows the angles measured observing $^{20}F$ decay. There are two clearly defined groups, the narrow group (FWHM=3°) is associated with electrons that come through the active collimator aperture while the broader (FWHM=20°) distribution is attributed to background. The ratio of signal to total counts at $B=1.625$ kG using these two approaches are $0.945\pm0.003$ and $0.938\pm0.002$. The spread in these values should be taken as the uncertainty in the background contribution for $^{20}F$ decay.

As mentioned earlier, the $^{20}F$ decay is used to determine the overall acceptance of the magnetic spectrograph. The acceptance is a product of three factors.

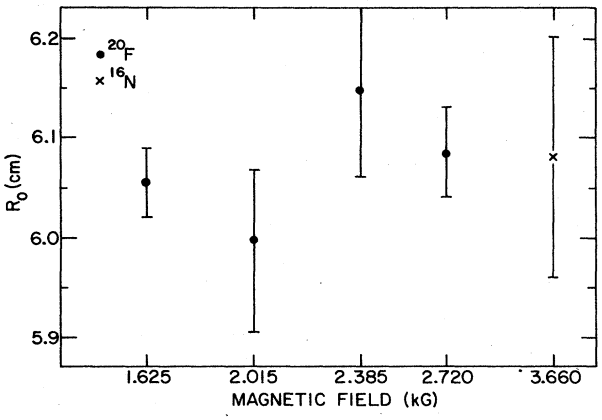


FIG. 9. The position offset $R_0$, as function of the magnetic field, determined from the fitting routine. A weighted mean gives $R_0=6.072\pm0.024$ cm.

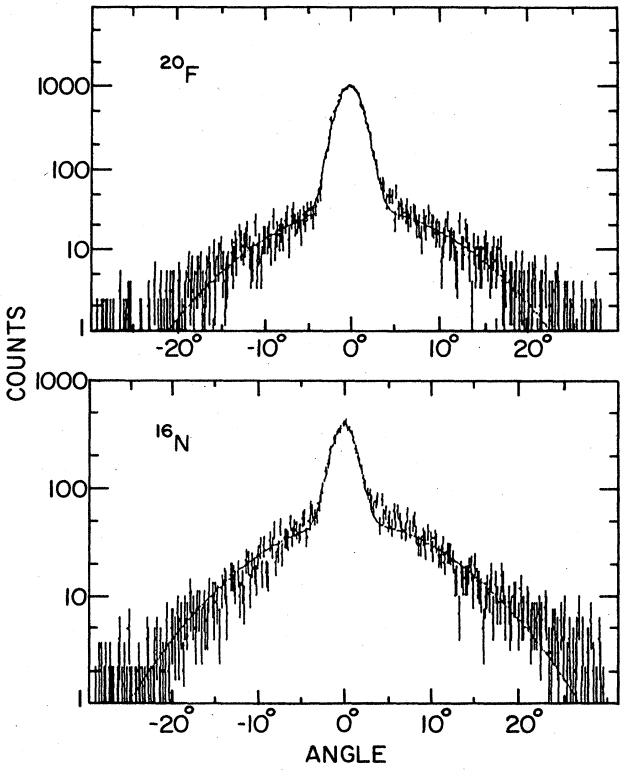


FIG. 10. The observed angles of the electron trajectories through the wire detector. The smooth curve is a two-Gaussian (six parameter) fit.

TABLE II. The overall efficiency of the spectrometer as a function of the magnetic field.

| Magnetic field (kG) | $\epsilon_{sp}\times 10^5$ |
|---|---|
| 1.625 | 3.794±0.05 |
| 2.015 | 4.02±0.14 |
| 2.385 | 3.71±0.22 |
| 2.720 | 4.00±0.27 |

$$\epsilon_{sp}=\frac{N(0,P_0)}{N(P_{min},P_{max})}\epsilon_0 d\Omega_{sp} .$$

The last factor $d\Omega_{sp}$ is the solid geometrical angle subtended by the spectrograph. The efficiency of the detector system is $\epsilon_0$. The ratio is the relative total spectrum to the faction between $p_{min}$ and $p_{max}$. Calculation of this ratio requires knowledge of the magnetic field ($B$), the spectrograph constant ($R_0$), and the spectral shape. A small correction is included to take account of weak magnetic effects on the spectrum of $^{20}$F.

Weighted mean of four measurements, shown in Table II, yields

$$\epsilon_{sp}=3.82\pm0.05\times10^{-5} .$$

Comparing this overall efficiency of the spectrometer to the acceptance solid angle of the active slit we find $\epsilon_0=93.4\%$. This is completely consistent with measurements of the efficiency of the wire detector, in which the efficiency for electron detection is $\sim 98\%$ for each of the three wire cells.

## IV. MEASUREMENT OF $^{16}$N GROUND STATE DECAY

Using the $^{20}$F results to calibrate the spectrometer, the branch to the $^{16}$O ground state in the decay of $^{16}$N can then be determined. The $^{16}$N activity was produced via the $^{15}$N(d,p)$^{16}$N reaction using a 1.7 MeV deuteron beam incident on a 99% $^{15}$N enriched melamine ($C_3H_6N_6$) target (300 $\mu$g/cm$^2$) on a carbon (40 $\mu$g/cm$^2$) backing. Au is evaporated on both sides (100 $\mu$g/cm$^2$ on the front and 150 $\mu$g/cm$^2$ on the back) to ensure that the recoiling $^{16}$N stop in the target.

The electron and gamma-ray singles spectra in this instance were found to consist of a component with proper time decay [($\tau=10.29$ sec) (Ref. 18) and a time independent component. A two-parameter fit to the data of the form $A\exp(-t/\tau_m)+B$, where $\tau_m$ is the decay time constant, determines the background present in the singles spectra. The higher background in the singles beta spectra for the $^{16}$N target is consistent with a larger carbon concentration in the target. In the case of the $\gamma$-ray spectrum, the background is greatly reduced due to the higher energy (6.13 MeV compared to 1.63 MeV) of the detected gamma ray. The time dependence of $\beta\gamma$ coincidences and of electrons detected in the magnetic spectrometer are again found to consist of only a single component with the proper decay time constant. The values for $A$ and $B$ are shown in Table I.

The $^{16}$N(2$^-$, g.s.) to $^{16}$O(0$^+$, g.s.) transition is unique first forbidden with a shape factor[23]

$$N(p)\propto p^2[E_0-\sqrt{p^2+1}]^2F(Z,p)[(E_0-\sqrt{p^2+1})^2+\lambda_2 p^2] .$$

The Fermi function $F(Z,p)$ and the electromagnetic correction factor $\lambda_2$ are taken from the tables of Behrens and Jänecke.[23] Figure 11 shows measured position spectra from the $^{16}$N decay. The background present in the position spectra is measured by using a 1.27 cm lead plate to block the entrance aperture of the spectrometer, and again using the electron angle through the wire detector to determine the background contribution. The measured angles and two-Gaussian fit to the data are shown in the bottom half of Fig. 10. At $B=2.720$ kG the ratio of signal to total counts for the two methods are 0.746±0.010 and 0.741±0.007, respectively. The background in the position spectra arises from the gamma rays penetrating into the spectrometer and generating electrons via Compton scattering or pair production which are deflected into the detection system.

Using the momentum calibration determined in the $^{20}$F decay and calculating the first forbidden unique shapes the fraction of the spectra observed in the spectrometer is determined. In every instance only the position of the $^{16}$N spectrum above the end point of the branch to the 6.13 MeV level is considered as shown in Fig. 11. The branching ratio is

$$\frac{\Gamma_\beta(2^-\rightarrow0^+)}{\Gamma_\beta(2^-)}=\frac{N(2^-\rightarrow0^+)}{N(2^-)}\epsilon_{sp} ,$$

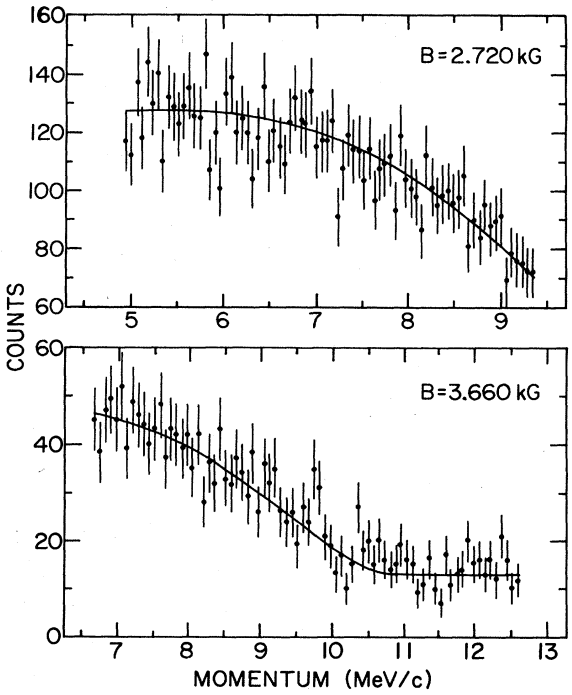


FIG. 11. Position spectra taken while observing $^{16}$N decays. The smooth curve is a two-parameter fit of the form

$$N(p)=A_0p^2[E_0-\sqrt{p^2+1}]^2F(Z,p)[(E_0-\sqrt{p^2+1})^2+\lambda_2p^2]+B_0.$$

where $N(2^-\rightarrow 0^+)$ is the number of $2^-\rightarrow 0^+$ electrons detected in the spectrometer, corrected for the fraction of the momentum spectrum accepted; $\epsilon_{sp}$ is the spectrometer efficiency already determined; and $N(2^-)$ is the total number of $^{16}N$ ground state decays. Two measurements of the branching ratio $\Gamma_\beta(2^-\rightarrow 0^+)/\Gamma_\beta(2^-)$ taken at 2.72 and 3.66 kG are, respectively, $0.2803\pm0.0070$ and $0.2856\pm0.0160$. The weighted mean of these two measurements yields a value

$$\frac{\Gamma_\beta(2^-\rightarrow 0^+)}{\Gamma_\beta(2^-)}=0.2811\pm0.0064$$

in excellent agreement with Ref. 19.

## V. APPLICATION OF THE RESULTS TO $^{16}N(0^-)$ DECAY

The excellent agreement between the values obtained above for $\Gamma_\beta(2^-\rightarrow 0^+)/\Gamma_\beta(2^-)$ and that determined in Ref. 19 ($0.279\pm0.005$) allows the two results to be combined. This produces a best value of

$$\frac{\Gamma_\beta(2^-\rightarrow 0^+)}{\Gamma_\beta(2^-)}=0.280\pm0.004\ .$$

Reference 19 also reports a precise value for

$$\frac{\Gamma_\beta(2^-\rightarrow 3^-)}{\Gamma_\beta(2^-)}=0.663\pm0.006\ .$$

Using this result and taking care to combine errors in a proper fashion one finds for a best value of

$$\frac{\Gamma_\beta(2^-\rightarrow 3^-)}{\Gamma_\beta(2^-\rightarrow 0^+)}=2.36\pm0.048\ .$$

As discussed in Sec. I all published experiments measuring the beta decay rate of the $^{16}N$, $0^-$, 120 keV level calibrated the efficiency of their beta detectors relative the $^{16}N$, $2^-$, ground state decay. In each case the calibration involved detecting the relative number of beta decays to the $^{16}O$ ground state relative to the number of 6.13 MeV $\gamma$ rays. Using the above result for $\Gamma_\beta(2^-\rightarrow 3^-)/\Gamma_\beta(2^-\rightarrow 0^+)$ we find for the ratio $R$, using results reported in Ref. 21,

$$R\equiv\frac{\text{Number of 6.13 MeV }\gamma\text{ rays}}{\text{Number of decays to }^{16}\text{O g.s.}}=2.386\pm0.049\ .$$

If this value for $R$ is used to generate the beta detector efficiency rather than the old value of $R=2.654\pm0.28$, a set of new values are generated for the beta branching ratio $B_\beta$ of the $^{16}N$, $0^-$, 120 keV level to the $^{16}O$ ground state. The best value is obtained by combining the results of Refs. 14, 16, and 24. This gives for the branching ratio

$$B_\beta=3.72\pm0.13\times10^{-6}$$

with a corresponding decay probability of

$$\Lambda_\beta(^{16}N,0^-,120\text{ keV}\rightarrow{}^{16}O,0^+,\text{ g.s.})=B_\beta/\tau_{0^-}\ ,$$

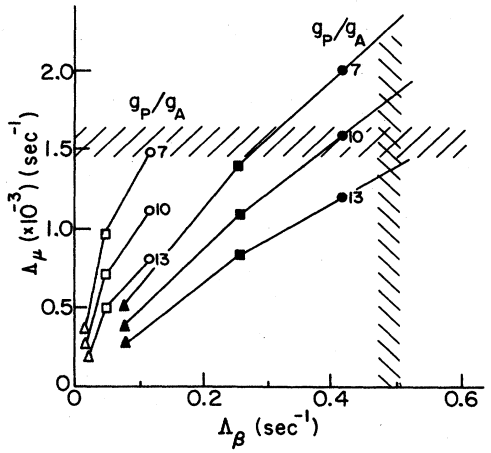


FIG. 12. The measured values of $\Lambda_\mu$ from Refs. 12 and 13 and $\Lambda_\beta$ from Refs. 16, 19, and 24 and the present work, along with the calculated values from Ref. 9. The open points are impulse-approximation calculations. The closed points include meson exchange currents in the weak Hamiltonian. In each case the calculation is done with three different residual interactions: a $\delta$ function plus $\pi$ and $\rho$ exchange (triangles), a $G$ matrix (squares), and a one-boson exchange potential (circles). Details regarding the residual interactions are specified in Ref. 9. The lines connecting the points are only meant to guide the eye.

where $\tau_{0^-}$ is the lifetime of the $^{16}N$, 120 keV level. Combining the value reported in Ref. 18 and the value $\tau_{0^-}=7.64\pm0.10$ $\mu$sec reported in Ref. 16 one has $\tau_{0^-}=7.61\pm0.07$ $\mu$sec. This directly leads to the result

$$\Lambda_\beta(^{16}N,0^-,120\text{ keV}\rightarrow{}^{16}O,0^+,\text{ g.s.})=0.489\pm0.02\text{ sec}^{-1}\ .$$

The most comprehensive calculation of $\Lambda$ $(0^+\leftrightarrow 0^-)$ in $A=16$ has been carried out by Towner and Khanna.[9] The points in Fig. 12 show the values of $\Lambda_\mu$ and $\Lambda_\beta$ calculated by Towner and Khanna. Results are shown both with and without the inclusion of meson exchange currents (MEC's). Three different residual interactions are used to compute the rate in order to check the model dependence of the result. The first interaction is a zero-range force, with one-pion and one-rho exchange added explicitly.[25] The second is a $G$ matrix derived from the Hamada-Johnston hard-core potential in a harmonic oscillator basis.[26] The third interaction is a one-boson exchange potential, including $\pi$, $\rho$, $\omega$, and $\sigma$ exchange terms.[9] The calculated values of $\Lambda_\beta$ and $\Lambda_\mu$ individually are seen to be sensitive to the choice of residual interaction. But the ratio $\Lambda_\mu/\Lambda_\beta$ is relatively insensitive to the interaction but is sensitive to the inclusion of meson exchange and the value of $g_p$, the pseudoscalar coupling constant.

The nucleons only impulse-approximation calculations (NOIA) of Ref. 9 are seen to underestimate $\Lambda_\beta$ by more than a factor of 3, independent of the residual interaction. This confirms the important role of pion exchange in the time component of the weak axial-vector current.

The measured ratio of $\Lambda_\mu/\Lambda_\beta$ would imply

$g_P/g_A \sim 12.5$ for the nucleon in this transition. Towner and Khanna calculate $\Lambda_\mu$ and $\Lambda_\beta$ to second order in perturbation theory using a harmonic oscillator basis that include all $2\hbar\omega$ excitations. Warburton and coworkers[19,27,28] suggested that radial wave functions generated in a finite potential could effect the result of these calculations. Thus, further theoretical work is needed to extract $g_p/g_A$ from these $N=16$ decays.

## ACKNOWLEDGMENTS

The authors would like to acknowledge the valuable assistance of Jordan Camp and David Wark in carrying out this experiment. Dr. J. Napolitano made several helpful suggestions in the preparation of this report. This research was supported by the U.S. Department of Energy under Contract No. W-31-109-Eng-38.

[1]K. Kubodera, A. Delorme, and M. Rho, Phys. Rev. Lett. **40**, 755 (1978).
[2]P. Guichon, M. Giffon, and C. Samour, Phys. Lett. **82B**, 28 (1978).
[3]P. Guichon, M. Giffon, J. Joseph, R. Laverriere, and C. Samour, Z. Phys. A **285**, 183 (1978).
[4]B. R. Holstein and C. W. Kim, Phys. Rev. C **19**, 1433 (1979).
[5]K. Koshigiri, H. Ohtsubo, and M. Morita, Prog. Theor. Phys. **62**, 706 (1979).
[6]W. K. Cheng, B. Lorazo, and B. Goulard, Phys. Rev. C **21**, 374 (1980).
[7]W. K. Cheng and B. Goulard, Phys. Rev. C **23**, 869 (1981).
[8]I. S. Towner and F. C. Khanna, in *Proceedings of the Ninth International Conference on High Energy Physics and Nuclear Structure, Versailles, 1981,* edited by P. Catillon, P. Radvanyi, and M. Porneuf (North-Holland, Amsterdam, 1982).
[9]I. S. Towner and F. C. Khanna, Nucl. Phys. **A372**, 331 (1981).
[10]J. Delorme, in *Proceedings of the Ninth International Conference on High Energy Physics and Nuclear Structure, Versailles, 1981,* edited by P. Catillon, P. Radvanyi, and M. Porneuf (North-Holland, Amsterdam, 1982).
[11]A. Maksymowicz, Nuovo Cimento **48A**, 320 (1967).
[12]F. R. Kane, M. Eckhause, G. H. Miller, B. L. Roberts, M. E. Vislay, and R. E. Welsh, Phys. Lett. **45B**, 292 (1973).
[13]P. Guichon, B. Ihoreau, M. Griffon, A. Concalves, J. Julien, L. Rowssel, and C. Semour, Phys. Rev. C **19**, 987 (1979).
[14]L. Palffy, J. P. Deutsch, L. Grenair, J. Lehmann, and M. Steels, Phys. Rev. Lett. **34**, 212 (1975).
[15]C. A. Gagliardi, G. T. Garvey, J. R. Wrobel, and S. J. Freedman, Phys. Rev. Lett. **48**, 914 (1982).
[16]C. A. Gagliardi, G. T. Garvey, J. R. Wrobel, and S. J. Freedman, Phys. Rev. C **28**, 2423 (1983).
[17]T. Minamisono, K. Tekoyana, T. Ishigai, H. Takeshima, Y. Nojiri, and K. Asahr, Phys. Lett. **130B**, 1 (1983).
[18]F. Ajzenberg-Selove, Nucl. Phys. **A375**, 1 (1982).
[19]E. K. Warburton, D. E. Alburger, and D. J. Millener, Phys. Rev. C **29**, 2281 (1984).
[20]D. E. Alburger, A. Gallman, and D. H. Wilkinson, Phys. Rev. **116**, 939 (1959).
[21]F. Ajzenberg-Selove, Nucl. Phys. **A392**, 1 (1983).
[22]Frank P. Calaprice and D. E. Alburger, **C17**, 730 (1978).
[23]H. Behrens and J. Jänecke, *Numerical Tables for Beta-Decay and Electron Capture* (Springer, Berlin, 1969).
[24]L. Lessard and L. A. Hamel (private communication).
[25]J. Speth, V. Klemt, J. Wambach, and G. E. Brown, Nucl. Phys. **A343**, 382 (1980).
[26]F. Herbert and B. R. Barrett, Nucl. Phys. **A254**, 13 (1975).
[27]D. J. Millener, D. E. Alburger, and E. K. Warburton, Phys. Rev. C **26**, 1167 (1982).
[28]D. J. Millener, J. W. Olness, and E. K. Warburton, Phys. Rev. C **28**, 497 (1983).